Integral Sliding Mode Control for Trajectory Tracking of a Quad-rotor UAV with Chattering Attenuation and External Wrenches Estimation

Domenico Tuccillo · Benito Vodola

https://github.com/BenitoVodola/QUAV_ISMC.git

https://github.com/DomenicoTuccillo/Final-project-FSR.git

Abstract—**The UAVs (Unmanned Aerial Vehicles) are aerial robots that operate without a human pilot on board and are controlled either autonomously by onboard computers or by remote control from a human operator. UAVs are classified with respect to the number of rotors they are composed of. In this thesis project we are going to examine a quad-copter with co-planar propellers, that is a nonlinear and underactuated system, that means the quad-copter robot cannot generate finite accelerations that allows the robot to move transversely without inclining its body. In this paper an improved integral sliding mode controller has been proposed and applied to track a desired trajectory.**

I. INTRODUCTION

The quad-rotor UAV has nonlinear dynamic equations, coupled and underactuated dynamics. Various control techniques are presented in literature to overcame these problems; in this paper we will present an improved version of Sliding Mode Control (SMC), which is a common non-linear control strategy, which pushes the system's dynamics towards a sliding surface in a finite time, in order to match certain requirements. The SMC is known to be a robust non-linear control strategy but with the drawback of presence of chattering in the control action. In this paper, an Integral Sliding Mode Control is proposed to improve the tracking capability of the UAV and, to reduce the chattering effect, the hyperbolic tangent is proposed as switching function. Furthermore, an estimator has been implemented to estimate the disturbances and uncertainties that affects the quad-rotor dynamics; through this computation we can improve the control laws with another contribution.

II. QUAV DYNAMIC MODEL

The QUAV moves in the space and exhibits six degrees of freedom (x,y,z,ϕ,θ,ψ), three for the position and three for the orientation, supposing of not being interested in the propellers' angles. The QUAV is composed by four propellers. Each one produces a thrust $T_i > 0$, this implies that the total thrust is $u_T = \sum_{i=1}^{4} T_i$

directed along the z_b axis of body frame to compensate the gravity and control the vertical motion. The frame we adopted to determine the pose of the QUAV is the *NED frame*, presented in the figure (1).
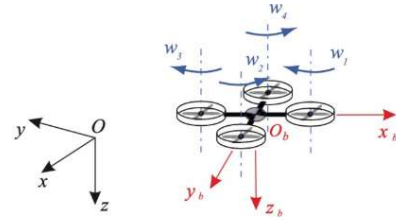

Figure 1: QUAV FRAME

The attitude is expressed through a minimal representation given by the *XYZ Euler Angles (roll-pitch-yaw)*, that we will denote as $\eta_b = \begin{bmatrix} \phi & \theta & \psi \end{bmatrix}^T \in \mathbb{R}^3$. Assuming that the vector of the generalized coordinates is:

$$q = \begin{bmatrix} p, \eta_b \end{bmatrix}^T \qquad (1)$$

where quad-rotor position is expressed in the world frame:

$$p_b = \begin{bmatrix} x, y, z \end{bmatrix}^T \in \mathbb{R}^3 \qquad (2)$$

and the quad-rotor orientation is:

$$\eta_b = \begin{bmatrix} \phi, \theta, \psi \end{bmatrix}^T \in \mathbb{R}^3 \qquad (3)$$

$$\begin{cases} m\ddot{p}_b = mge_3 - u_T R_b e_3 + f_e \\ M(\eta_b)\ddot{\eta}_b = -C(\eta_b,\dot{\eta}_b)\dot{\eta}_b + Q^T(\eta_b)\tau^b + Q^T(\eta_b)\tau_e^b \end{cases}$$

$$(4)$$

where

- $M(\eta_b) = Q^T(\eta_b)I_b Q(\eta_b) \in \mathbb{R}^{3\times3}$ is a symmetric and positive definite matrix provided that $\theta \neq \frac{\pi}{2}$;
- $C(\eta_b,\dot{\eta}_b) = Q^T(\eta_b)S(Q(\eta_b)\dot{\eta}_b)I_b Q(\eta_b) + Q^T(\eta_b)I_b\dot{Q}(\eta_b) \in \mathbb{R}^{3\times3}$ with $S(\cdot) \in \mathbb{R}^{3\times3}$ the skew-symmetric operator;
- $Q(\eta_b) \in \mathbb{R}^{3\times3}$ is the transformation matrix such that $\omega_b^b = Q(\eta_b)\dot{\eta}_b$ and is equal to:

$$\begin{bmatrix} 1 & 0 & -s_\theta \\ 0 & c_\phi & c_\theta s_\phi \\ 0 & s_\phi & c_\theta c_\phi \end{bmatrix}$$

- $e_3 = \begin{bmatrix} 0 & 0 & 1 \end{bmatrix}^T$;
- $R_b(\eta_b) \in SO(3)$ is the rotation matrix of body frame with respect to the world frame and is equal to:

$$\begin{bmatrix} c_\theta c_\psi & s_\phi s_\theta c_\psi - c_\phi s_\psi & c_\phi s_\theta c_\psi + s_\phi s_\psi \\ c_\theta s_\psi & s_\phi s_\theta s_\psi + c_\phi c_\psi & c_\phi s_\theta s_\psi - s_\phi c_\psi \\ -s_\theta & s_\phi c_\theta & c_\phi c_\theta \end{bmatrix}$$

- $I_b \in \mathbb{R}^{3\times3}$ is the diagonal inertia matrix for the angular part and referred to the body frame;
- m is the mass of the QUAV and it is positive definite;
- $f_e^b, \tau_e^b \in \mathbb{R}^r$ external or unmodelled terms expressed in the body frame;
- u_T, τ^b are the control inputs of the QUAV, but the real inputs are the velocity for each propeller.

With reference to the figure 1, if we assume:

- $l > 0$ the distance of each propeller to the QUAV's centre;
- Q_i the fan torque due to air drag;
- $T_i = c_T\omega_i^2$, with $c_T > 0$ the thrust constant;
- $Q_i = c_Q\omega_i^2$, with $c_Q > 0$ the drag factor;

we can compute the sought relation:

$$\begin{bmatrix} u_T \\ \tau_x \\ \tau_y \\ \tau_z \end{bmatrix} = \begin{bmatrix} c_T & c_T & c_T & c_T \\ 0 & -lc_T & 0 & lc_T \\ lc_T & 0 & -lc_T & 0 \\ -c_Q & c_Q & -c_Q & c_Q \end{bmatrix} \begin{bmatrix} \omega_1^2 \\ \omega_2^2 \\ \omega_3^2 \\ \omega_4^2 \end{bmatrix} \quad (5)$$

III. TRAJECTORY PLANNING

We recall the differential flatness definition: *An affine control system is differentially flat if and only if there exists a flat output, continuous and differentiable, such that it is possible to express the state and the input as a function of the flat output and its time derivatives*; through the flat outputs it is possible to retrieve the full behavior of the system and it is useful for the explicit trajectory generation. The QUAV's flat outputs are the variables x,y,z,ψ, so these are the ones that can be

actually planned. The initial conditions of the QUAV are: $q_0 = \begin{bmatrix} 0 & 0 & -2 & 0 & 0 & 0 \end{bmatrix}^T$.

1) TIME LAW: The desired trajectory has been split into two parts: the geometric path $q(s)$ such that $\frac{dq(s)}{ds} \neq 0 \ \forall s \in \mathbb{R}$, and the time law $s(t)$ such that $\dot{s} > 0 \ \forall t \in [t_i, t_f]$. First, the time law has been chosen as a seventh-order polynomial, in order to guarantee the jerk's continuity. Once s, $\dot{s}$, $\ddot{s}$ and $\dddot{s}$ have been computed, we impose $s_i = 0$, $s_f = 1$, $\dot{s}_i = 0$, $\dot{s}_f = 0$, $\ddot{s}_i = 0$, $\ddot{s}_f = 0$, $\dddot{s}_i = 0$, $\dddot{s}_f = 0$, regardless of the geometric path that will be selected.

2) GEOMETRIC PATH: Then the desired trajectory has been computed using motion primitives. The selected trajectory is composed of three different parts: a first helix, which projected on the yz plane gives a circle; a rectilinear path and a second helix, which projected in the xy plane gives a circle. Regarding the rectilinear path, the following path primitive has been employed:

$$\begin{aligned} p(s) &= (1-s)p_i + sp_f \\ \dot{p} &= (p_f - p_i)\dot{s} \\ \ddot{p} &= (p_f - p_i)\ddot{s} \\ \dddot{p} &= (p_f - p_i)\dddot{s} \end{aligned}$$

$$(6)$$

It is common practice to parameterize the trajectory using a curvilinear abscissa which varies from 0 to $||p_f - p_i||$. The path primitive for a straight line segment is often defined as:

$$p(s) = p_i + \frac{s}{||p_f - p_i||}(p_f - p_i) \quad (7)$$

However, we have opted for a different parametrization, where $s_i = 0$ and $s_f = 1$, utilizing the path primitive in equation (6). There are several reasons for this choice:

1) **Simplification of Parameters**: By setting $s \in [0,1]$, the parametrization has been normalized. This simplifies calculations and makes the interpretation of s more intuitive, as it directly represents the progression from the initial point $\mathbf{p}_i$ to the final point $\mathbf{p}_f$.
2) **Uniformity and Consistency**: Using a normalized parameter s ranging from 0 to 1 ensures a consistent approach across different segments of the trajectory. This uniformity can be advantageous when implementing complex trajectories involving multiple segments, as it avoids the need to rescale s for each segment.
3) **Ease of Implementation**: The chosen path primitive 6 is mathematically simpler to implement. It eliminates the need to compute $||\mathbf{p}_f - \mathbf{p}_i||$ and the

corresponding division, which can be computation-ally beneficial, especially in real-time applications.

In conclusion, while the traditional approach with the curvilinear abscissa is effective, the normalized parameter s provides several practical advantages in terms of simplicity, consistency, and ease of implementation. This approach ensures that the trajectory planning is straightforward and computationally efficient, which is particularly beneficial in robotics applications, where real-time performance is critical. To describe the path primitive of a helix in the yz plane, consider the initial position $\mathbf{p}_0 = (x_0, y_0, z_0)$. The coordinates for center position are defined as follows:

$$
\begin{aligned}
p_{Cx} &= x_0 \\
p_{Cy} &= y_0 + \rho \\
p_{Cz} &= z_0
\end{aligned}
\tag{8}
$$

The trajectory of the spiral is parameterized by s. The position coordinates as a function of s are given by:

$$
\begin{aligned}
p_{dx} &= (1-s)p_{Cx} + s(p_{Cx} + d) \\
p_{dy} &= p_{Cy} - \rho \cos(\alpha s) \\
p_{dz} &= p_{Cz} - \rho \sin(\alpha s)
\end{aligned}
\tag{9}
$$

In this formulation:

- p_{dx} represents the x-coordinate, which linearly interpolates between x_0 and $x_0 + d$.
- p_{dy} and p_{dz} describe a circular motion in the yz plane, centered at $(y_0 + \rho, z_0)$, with ρ being the radius of the circle and α being a constant that determines the angular frequency of the helix.

This parametrization ensures that the trajectory transitions smoothly from the initial position to the final position while tracing the helix path. **The linear interpolation in the x-direction combined with the circular motion in the yz plane creates a helical trajectory**. The derivatives in Equation (9) have been omitted for simplicity but they have been planned up to the jerk.
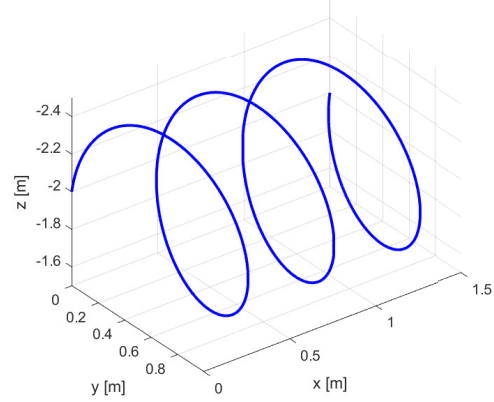
Figure 2: First Helix

Analogously, a similar parametrization can be done for the helix in the xy plane.
Regarding the yaw desired trajectory, it was computed as a rectilinear path between some angles, using Equation (6). To fully evaluate the steady state for each part it has been also planned a dead time between each trajectory, in which the UAV stays still. The values of desired angles, the duration of each part and the geometric parameters have been encapsulated in the following tabels:

Parameter	Symbol	Value	Unit
Distance along x	d	1.5	m
Angular frequency	α	6π	rad/s
Radius	ρ	0.5	m
Duration	t_f	40	s
Dead time	t_{dead}	15	s
Desired Yaw	ψ_d	$\pi/4$	rad

Table I: Parameters for the first path

Parameter	Symbol	Value	Unit
Distance along x	x_d	1	m
Distance along y	y_d	1	m
Distance along z	z_d	1	m
Duration	t_f	20	s
Dead time	t_{dead}	10	s
Desired Yaw	ψ_d	-0.3491	rad

Table II: Parameters for the second path

Parameter	Symbol	Value	Unit
Distance along z	d	1.5	m
Angular frequency	α	3π	rad/s
Radius	ρ	0.75	m
Duration	t_f	40	s
Dead time	t_{dead}	25	s
Desired Yaw	ψ_d	$3\pi/2$	rad

Table III: Parameters for the third path

In the next figures are reported: the final composed trajectory, alongside its derivatives and the 3D plot of the final trajectory.
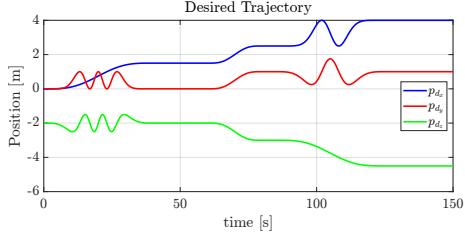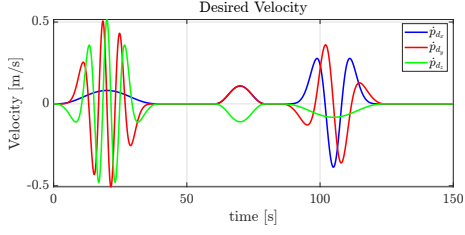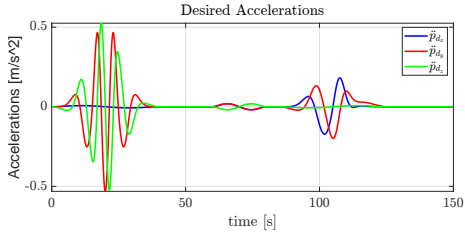
Figure 3: Desired Positions

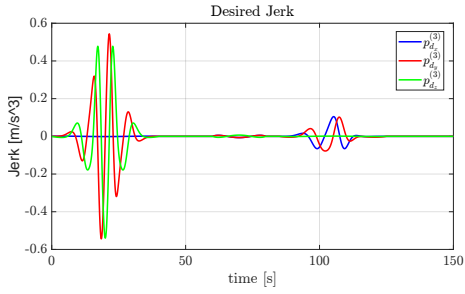Figure 4: Desired Velocities

Figure 5: Desired Accelerations

Figure 6: Desired Jerks
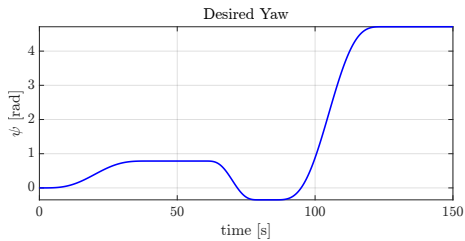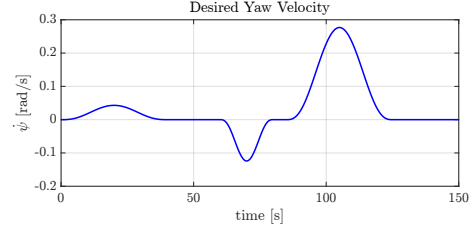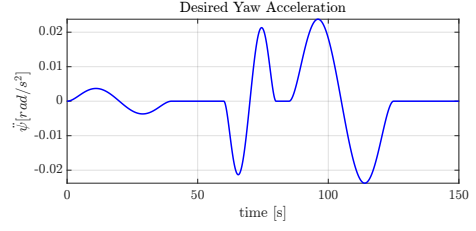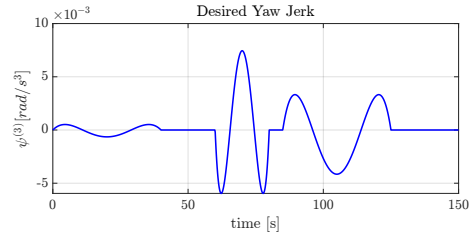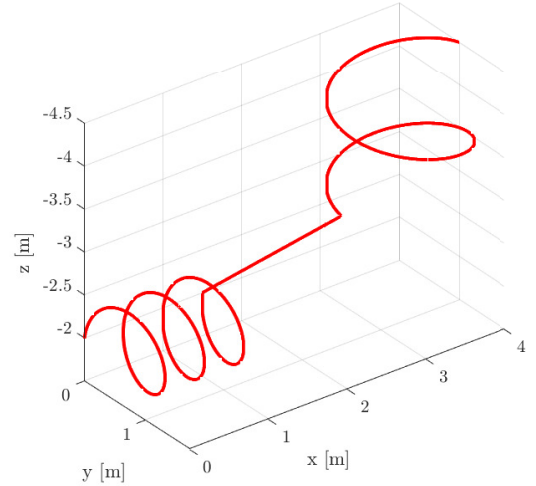

Figure 7: Desired ψ

Figure 8: Desired $\dot{\psi}$

Figure 9: Desired $\ddot{\psi}$

Figure 10: Desired $\dddot{\psi}$

Figure 11: Desired Trajectory

IV. CONTROL SYNTHESIS

In this section we are going to discuss the proposed control algorithm design. The whole controller is com-

posed by: the inner loop control whose aim is to stabilize the QUAV attitude, and the outer loop control which is responsible for the stability of the position.

A. INNER LOOP SYNTHESIS

The control objective is to design an ISMC control law to stabilize the error dynamics of the QUAV attitude and to bring it to the suitable sliding surface. Recalling the equation (4) the dynamic equation of the orientation is:

$$M(\eta_b)\ddot{\eta}_b = -C(\eta_b, \dot{\eta}_b)\dot{\eta}_b + Q^T(\eta_b)\tau^b + Q^T(\eta_b)\tau_e^b \quad (10)$$

Assuming the error on the attitude and its time derivative as follows:

$$e_\eta = \eta_b - \eta_{b,d} \quad (11)$$

$$\dot{e}_\eta = \dot{\eta}_b - \dot{\eta}_{b,d} \quad (12)$$

where η_b is the measured roll, pitch and yaw angles vector, instead η_d is the desired roll, pitch and yaw angles vector; the sliding surface has been chosen as:

$$\sigma_\eta = \dot{e}_\eta + K_{1\eta}e_\eta + K_{2\eta}\int_0^t e_\eta d\tau \quad (13)$$

where $\sigma_\eta = \begin{bmatrix} \sigma_\phi & \sigma_\theta & \sigma_\psi \end{bmatrix}^T$ represents the vector of the three sliding surfaces; instead, $K_{1\eta}$ and $K_{2\eta}$ are two diagonal positive definite matrices and they represent the control gains. In order to guarantee attractivity of the selected sliding surface, the time derivative of (13) must be:

$$\dot{\sigma}_\eta = -\lambda_{1\eta}sgn(\sigma_\eta) - \lambda_{2\eta}\sigma_\eta \quad (14)$$

where $\lambda_{1\eta}$ and $\lambda_{2\eta}$ are diagonal positive definite matrices. Substituting the (11) into (13) and time differentiating we obtain:

$$\dot{\sigma}_\eta = (\ddot{\eta}_b - \ddot{\eta}_d) + K_{1\eta}\dot{e}_\eta + K_{2\eta}e_\eta \quad (15)$$

Then, substituting the attitude dynamics (10) into the (15) and imposing that (15) and (14) are equal, the control inputs must be:

$$\tau^b = Q^{-T}M(\ddot{\eta}_d + M^{-1}C\dot{\eta}_b - K_{2\eta}e_\eta - K_{1\eta}\dot{e}_\eta$$
$$- \lambda_{1\eta}sgn(\sigma_\eta) - \lambda_{2\eta}\sigma_\eta) - Q^{-T}\hat{\tau}_e^b \quad (16)$$

where $\hat{\tau}_e^b$ is the contribution of the estimation of the disturbances acting on the system. To reduce the chattering the $sign(\sigma_\eta)$ has been approximated by the hyperbolic tangent function. Notice that it is almost the same control law used in the classical hierarchical controller, but enhanced with a sliding action that make it more robust.

B. ATTRACTIVITY AND STABILITY PROOF

The attractivity condition of the selected sliding surface, which is the reason why it was imposed the (14), can be proven by selecting the candidate Lyapunov function as:

$$V(\sigma_\eta) = \frac{1}{2}\sigma_\eta^T\sigma_\eta \quad (17)$$

By differentiating the (17) with respect to the time:

$$\dot{V} = \sigma_\eta^T\{-\lambda_{1\eta}sgn(\sigma_\eta) - \lambda_{2\eta}\sigma_\eta\} =$$
$$= -\sigma_\eta^T\lambda_{1\eta}sgn(\sigma_\eta) - \lambda_{2\eta}\sigma_\eta^T\sigma_\eta =$$
$$= -\lambda_{1,\phi}|\sigma_\phi| - \lambda_{1,\theta}|\sigma_\theta| - \lambda_{1,\psi}|\sigma_\psi| -$$
$$\lambda_{2,\phi}\sigma_\phi^2 - \lambda_{2,\theta}\sigma_\theta^2 - \lambda_{2,\psi}\sigma_\psi^2 \quad (18)$$

Where the (14) has been employed.
From the (18) we can state that the $\dot{V} < 0 \; \forall\sigma_\eta \in \mathbb{R}^n, \sigma_\eta \neq 0$, if $\lambda_{1\eta}$ and $\lambda_{2\eta}$ are diagonal positive definite matrices; so for the Lyapunov direct method the sliding surface is attractive. Thus, the (14) is zero when we are on the sliding surface, that is $\sigma_\eta = 0$. But, since the dynamics on the sliding surface is also given by (15) it must be that:

$$\ddot{e}_\eta + K_{1\eta}\dot{e}_\eta + K_{2\eta}e_\eta = 0 \quad (19)$$

which is a linear homogeneous second order differential equation and in such way, since $K_{1\eta}$ and $K_{2\eta}$ are diagonal and positive definite, the errors converge to zero asymptotically. Thus, both attractivity and stability are proven.

C. OUTER LOOP SYNTHESIS

As for the inner loop controller, we want to design a controller based on the integral sliding mode control to stabilize the quad-copter position. Considering the position dynamics:

$$m\ddot{p}_b = mge_3 - u_T R_b e_3 \quad (20)$$

Recalling the tracking error for the attitude (11) and its time derivative (12); consider the following definition, forgetting for now that the system is underactuated, that is like the virtual desired acceleration oriented as the desired attitude, regulated by the total thrust, plus gravity:

$$\mu_d = \begin{bmatrix} \mu_x & \mu_y & \mu_z \end{bmatrix}^T = -\frac{1}{m}u_T R_b(\eta_{b,d})e_3 + ge_3 \quad (21)$$

where $\eta_b = e_\eta + \eta_{b,d}$ from the equation (11). If we substitute this expression into $R_b(\eta_b)$ of (20) we obtain:

$$\ddot{p}_b = \mu_d + \frac{1}{m}\delta(\eta_{b,d}, e_\eta) \quad (22)$$

Where $\delta(\eta_{b,d}, e_\eta)$ is the interconnection term between the linear and the angular part, which is strictly nonlinear. The outer loop controller can be designed as a PD action with a feed-forward action as:

$$\mu_d = -K \begin{bmatrix} e_p \\ \dot{e}_p \end{bmatrix} + \ddot{p}_{b,d} \tag{23}$$

As for the classical hierarchical controller, to show the asymptotic stability of the errors equal to zero, the interconnection term requires the use of perturbation theory, in order to prove that it is bounded in the transient. However, it vanishes if the error angular part goes to zero, which means that the attitude dynamics should be faster than the position one. Now, assuming we make the angular part faster, we would like to add a sliding action also in the outer loop formulation and prove the attractivity, as for the attitude. If we consider vanished the interconnection term, (22) becomes:

$$\ddot{p}_b = \mu_d \tag{24}$$

Let's define the error dynamics for the QUAV position as follows:

$$\begin{aligned} e_p &= p_b - p_{b,d} \\ \dot{e}_p &= \dot{p}_b - \dot{p}_{b,d} \end{aligned} \tag{25}$$

where p_b is the measured position vector, instead $p_{b,d}$ is the desired position vector; the sliding surface has been chosen as:

$$\sigma_p = \dot{e}_p + K_{1p}e_p + K_{2p}\int_0^t e_p d\tau \tag{26}$$

where $\sigma_p = \begin{bmatrix} \sigma_x & \sigma_y & \sigma_z \end{bmatrix}^T$ represents the vector of the three sliding surfaces; instead, K_{1p} and K_{2p} are two diagonal positive definite matrices and they represent the control gains. Then, the sliding mode dynamics has been chosen as follows, similar to the one chosen for the inner loop:

$$\dot{\sigma}_p = -\lambda_{1p}sgn(\sigma_p) - \lambda_{2p}\sigma_p \tag{27}$$

where λ_{1p} and λ_{2p} are diagonal positive definite matrices. Substituting the (25) into (26) and time differentiating we obtain:

$$\dot{\sigma}_p = (\ddot{p}_b - \ddot{p}_{b,d}) + K_{1p}\dot{e}_p + K_{2p}e_p \tag{28}$$

Then, substituting the position dynamics (24) into the (28) and imposing that (28) and (27) are equal, the control inputs must be::

$$\begin{aligned} \mu_d = &- \begin{bmatrix} K_{2p} & K_{1p} \end{bmatrix} \begin{bmatrix} e_p \\ \dot{e}_p \end{bmatrix} \\ &+ \ddot{p}_d - \lambda_{1p}sgn(\sigma_p) - \lambda_{2p}\sigma_p \end{aligned} \tag{29}$$

To reduce the chattering the $sgn(\sigma_p)$ has been approximated by the hyperbolic tangent function.
The attractivity proof for the position sliding surface is omitted because it results to be identical to the proof of attitude sliding surface.

In such way attractivity is proved just when the interconnection term is vanished, the complete stability proof still needs the use of perturbation theory. Furthermore, (29) can be enhanced with an external force estimation action $\hat{f}_e$ and can be modified as follows:

$$\begin{aligned} \mu_d = &- \begin{bmatrix} K_{2p} & K_{1p} \end{bmatrix} \begin{bmatrix} e_p \\ \dot{e}_p \end{bmatrix} \\ &+ \ddot{p}_d - \lambda_{1p}\tanh(\sigma_p) - \lambda_{2p}\sigma_p - \frac{\hat{f}_e}{m} \end{aligned} \tag{30}$$

We can compute the desired thrust and attitude from (21) through the flat outputs:

$$u_T = m\sqrt{\mu_x^2 + \mu_y^2 + (\mu_z - g)^2} \tag{31}$$

and,

$$\begin{aligned} \phi_d &= \sin^{-1}\left(\frac{m}{u_T}(\mu_y \cos\psi_d - \mu_x \sin\psi_d) \right) \\ \theta_d &= \tan^{-1}\left(\frac{\mu_x \cos\phi_d + \mu_y \sin\phi_d}{\mu_z - g} \right) \end{aligned} \tag{32}$$

D. MOMENTUM-BASED ESTIMATOR SYNTHESIS

The momentum-based estimator of order r has been proposed as the solution to estimate disturbances acting on the QUAV during the flight. Through the computation of the momentum vector q :

$$q = \begin{bmatrix} mI_3 & 0_3 \\ 0_3 & M(\eta_b) \end{bmatrix} \begin{bmatrix} \dot{p}_b \\ \dot{\eta}_b \end{bmatrix} \tag{33}$$

Then, the estimator of order r can be chosen as:

$$G_i(s) = \frac{c_0}{s^r + c_{r-1}s^{r-1} + ... + c_1 s + c_0} \tag{34}$$

The order of the filter and its coefficients $c_1, c_2 \ldots c_n$ are reported in the table [VII]. Once obtained these coefficients, first we have to compute the gains for the estimation:

$$\prod_{i=j+1}^{r} K_i = c_j, \quad j = 0, ..., r-1 \tag{35}$$

Then, the estimation law is:

$$\gamma_1 = K_1 q - K_1 \int_0^t \begin{bmatrix} \hat{f}_e \\ \hat{\tau}_e \end{bmatrix} + \begin{bmatrix} mge_3 - u_T R_b e_3 \\ C^T(\eta_b, \dot{\eta}_b)\dot{\eta}_b + Q^T(\eta_b)\tau^b \end{bmatrix} dt \tag{36}$$

$$\gamma_i = K_i \int_0^t - \begin{bmatrix} \hat{f}_e \\ \hat{\tau}_e \end{bmatrix} + \gamma_{i-1} dt, \quad i = 2, ..., r \tag{37}$$

With this estimator we can compute the term $\hat{\tau}_e^b$ in the equation (16) and $\hat{f}_e^b$ in the equation (30) to improve the performances of our controller. It is essential to highlight that the sliding mode controller is already able to manage the disturbances and the uncertainties due to its robustness; however, the momentum-based estimator

has been considered because it is able to provide the estimation of the disturbances and uncertainties that affect the system.

V. SIMULATION

A. MODEL PARAMETERS

The proposed parameters have been inspired by [1].

Parameter	Symbol	Value	Unit
Mass	m	6.5×10^{-1}	Kg
Inertia on x-axis	I_x	7.5×10^{-3}	$Kg \cdot m^2$
Inertia on y-axis	I_y	7.5×10^{-3}	$Kg \cdot m^2$
Inertia on z-axis	I_z	1.3×10^{-2}	$Kg \cdot m^2$
Thrust coefficient	c_T	3.13×10^{-5}	$N \cdot s^2/rad^2$
Drag coefficient	c_Q	7.5×10^{-7}	$N \cdot m \cdot s^2/rad^2$
Arm Length	l	2.3×10^{-1}	m

Table IV: Physical parameters

Parameter	ϕ	θ	ψ
$\lambda_{1\eta}$	1	1	1
$\lambda_{2\eta}$	5	5	5
$K_{1\eta}$	220	200	250
$K_{2\eta}$	100	100	100

Table V: Inner Loop parameters

Parameter	x	y	z
λ_{1p}	1	1	1
λ_{2p}	5	5	5
K_{1p}	200	200	200
K_{2p}	100	100	150

Table VI: Outer Loop parameters

Parameter	Value
r	1
c_0	100

Table VII: Filter parameters

The parameters of table [V], [VI] and [VII] have been obtained by trial and error procedure.
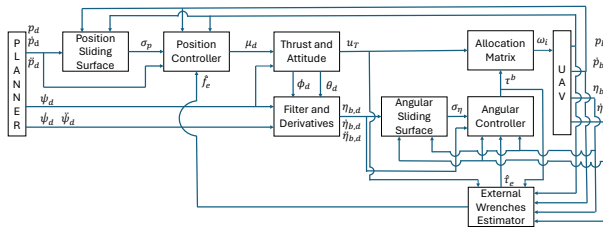
Figure 12: Control scheme

B. SIMULATION RESULTS

The controller's tracking ability is initially evaluated in an ideal environment, free from disturbances or uncertainties. This step is crucial for establishing a baseline and understanding the intrinsic performance of the controller. Subsequently, disturbances and uncertainties are introduced to simulate real-world conditions, in order to assess the controller's robustness. This allows for the analysis of the controller performance under unmodelled dynamics. Finally, a disturbance estimator is implemented, aimed at mitigating the impact of disturbances and enhancing the overall performance of the system. This approach simplifies the development of a more robust and reliable controller for practical applications.

1) ISMC: In this scenario an ideal environment with neither uncertainties nor disturbances has been considered. From the figures below we can state that the proposed controller exhibits a remarkable behavior, indeed, by looking at the errors figures (14), (16), (18), (20) we observe that the trajectory is perfectly tracked with very small errors. Furthermore, from the errors plot we can observe that the most critical portion of the path is the first helix (first 20 seconds), where the errors tend to increase given the complex trajectory which requires the pose vector to evolve within a small amount of time, since also the attitude has to evolve alongside the position. The angular velocities of the four propellers have been computed with a suitable allocation matrix, according to the convention in Figure 1, and reverting (5) we can compute:

$$\begin{bmatrix} \omega_1^2 \\ \omega_2^2 \\ \omega_3^2 \\ \omega_4^2 \end{bmatrix} = \begin{bmatrix} c_T & c_T & c_T & c_T \\ 0 & -lc_T & 0 & lc_T \\ lc_T & 0 & -lc_T & 0 \\ -c_Q & c_Q & -c_Q & c_Q \end{bmatrix}^{-1} \begin{bmatrix} u_T \\ \tau_x \\ \tau_y \\ \tau_z \end{bmatrix} \quad (38)$$

According to the selected frame (1), ω_1 and ω_3 will be negative since the associated propellers spin is clockwise, while ω_2 and ω_4 will be positive; in Figure (24) these velocities are plot, notice that they are all positive since it was decided to plot the norm.

2) ISMC WITH UNCERTAINTY: Here, it has been proposed the case in which the system is affected by an uncertainty on the QUAV's mass of fifty percent, so the real mass will be raised from $0.650Kg$ up to $0.975Kg$. From the control theory about SMC, with a sufficient big gain on the control action, the controller will be robust with respect to the uncertainty. From the figure (25), (26), (27), (28) indeed, we can state that even if the system has a considerable uncertainty, the controller is still able to track the trajectory with sufficiently small errors, but we can appreciate a small transient along the z-component of the position error; moreover, from the figures (29) and (30) we can appreciate the differences in the control inputs and the velocities of each propeller:
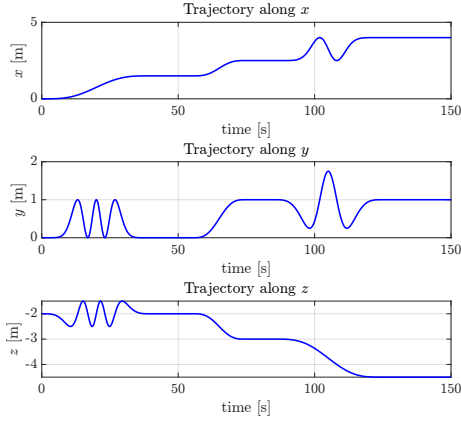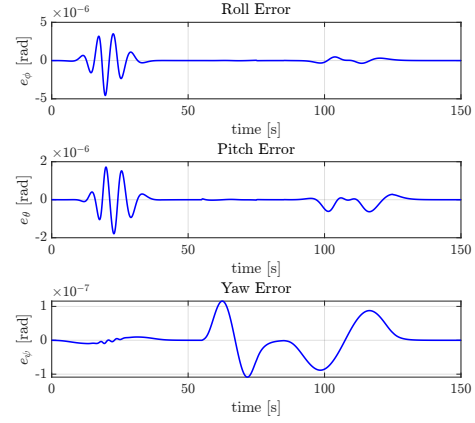
Figure 13: Measured Linear Positions

Figure 14: Linear Position Error
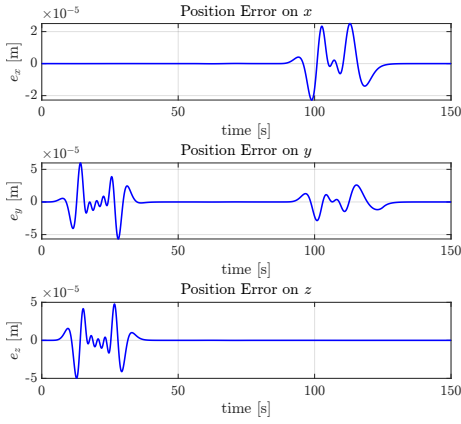

Figure 15: Measured Roll, Pitch, Yaw

Figure 16: Roll, Pitch, Yaw Errors
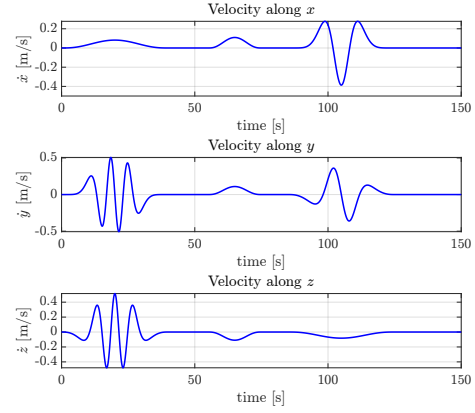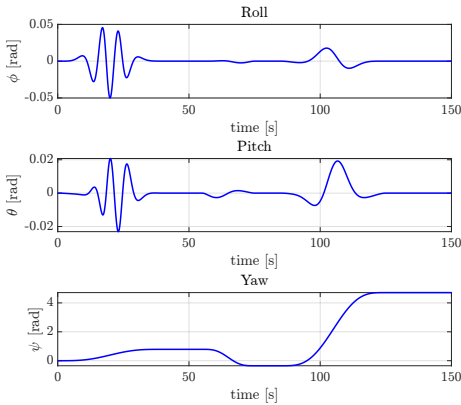

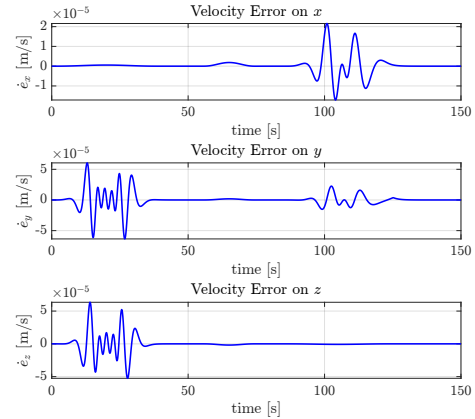Figure 17: Measured Linear Velocity

Figure 18: Linear Velocity Error

the initial thrust results much higher than the previous case in Figure (23) and the propellers exhibit a distinct transient and bigger rotation velocities than the (24), since now the UAV is heavier than before. Although this big uncertainty on the mass, the tracking capability are quite good, despite the initial transient, showing that the designed controller is, indeed, robust to parametric

uncertainties, as one can expect from a SMC based control.

3) ISMC + ESTIMATOR WITH UNCERTAINTIES: The next step is to analyze the behavior of the controller by adding the contribution provided the momentum-based estimator. As said before, the advantage of using an estimator is to provide the estimation of the uncertain-
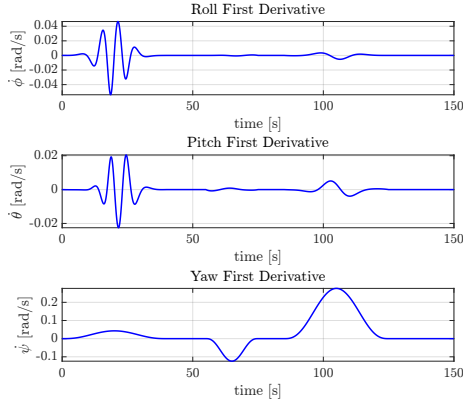
Figure 19: Measured Roll, Pitch, Yaw First Derivative

Figure 20: Roll, Pitch, Yaw First Derivatives Error

Figure 21: Measured Linear Acceleration

Figure 22: Measured Roll, Pitch, Yaw Second Derivatives

Figure 23: Control Inputs
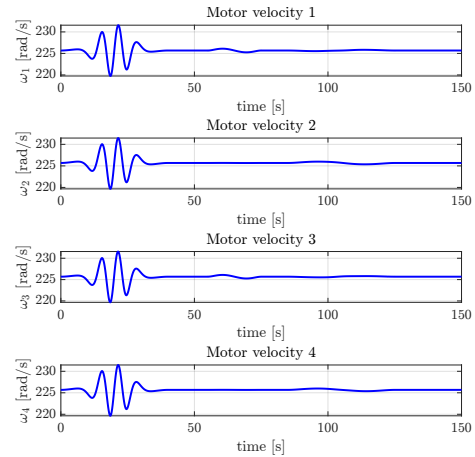
Figure 24: Norm of Propellers velocities

ties and disturbances, and compensate for them clearly. It is essential to highlight that the estimator dynamics can affect the system behaviour. From the figures (31), (32), (33), (34) the transient of the pose error exhibits a smaller peak value than the case without the estimator (see figures (25), (26), (27), (28)), indeed, we have reduced the peak for the third component of position error from $3 \cdot 10^{-3}m$ to $20 \cdot 10^{-5}m$. Furthermore, the peak of the third component of the linear velocity error is reduced from $2 \cdot 10^{-2}m/s$ to $1 \cdot 10^{-2}m/s$. Instead,
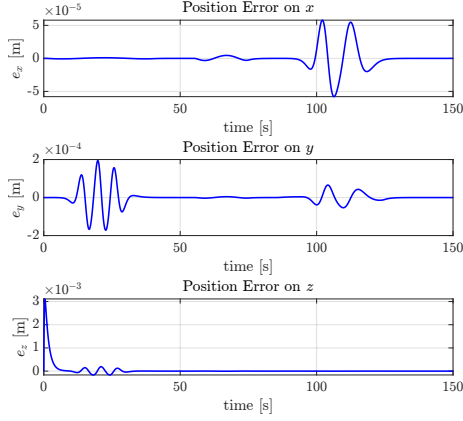
Figure 25: Linear Position Error With Uncertainty

Figure 26: Roll, Pitch, Yaw Errors With Uncertainty
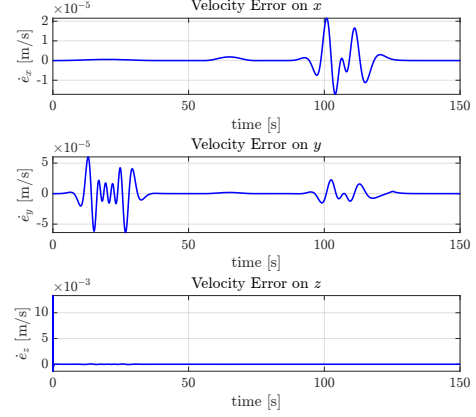

Figure 27: Linear Velocity Error With Uncertainty

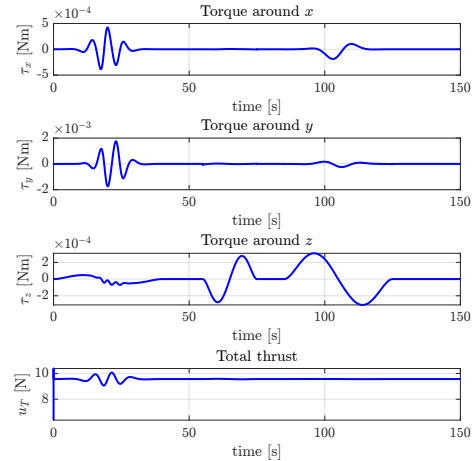Figure 28: Roll, Pitch, Yaw First Derivatives Error With Uncertainty

Figure 29: Control Inputs With Uncertainty
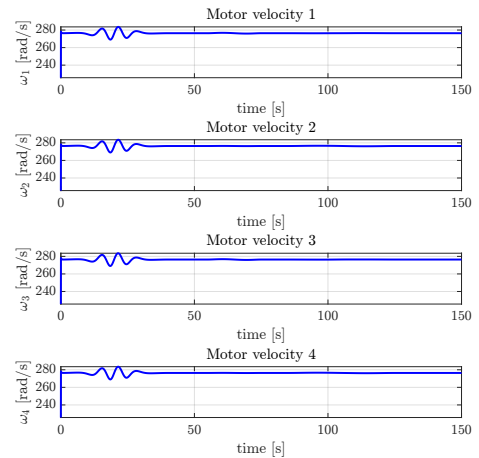
Figure 30: Norm of Propellers velocities With Uncertainty

the control inputs and propellers velocity behaviors are similar to the case without the estimator, while the errors on Euler angles exhibit a worse behavior than the case without the estimator; this is due to the estimator dynamics, which computes some values different from zero, but very small, that are comparable with such small errors and interfere with it, see Figure (38). Moreover,

we can appreciate the performances of the estimator from the figures (37) and (39), indeed, the mass estimation has

been obtained almost instantaneously with the following relationship:

$$mass_{real} = mass + \frac{\hat{f}_{e,z}}{\ddot{p}_{b,z} + g} \quad (39)$$

But, in the figure (39), a relevant oscillation of the mass estimation appears, this due to the complex trajectory and estimator dynamics during the first helix path.
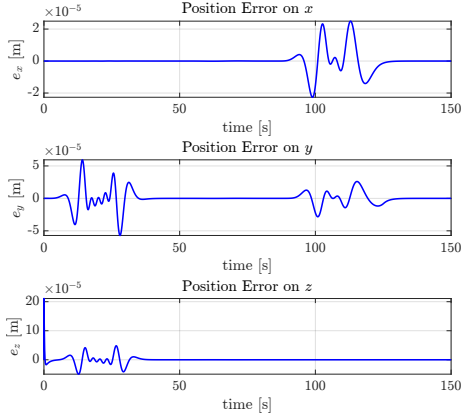
Figure 31: Linear Position Error With Uncertainty Compensated
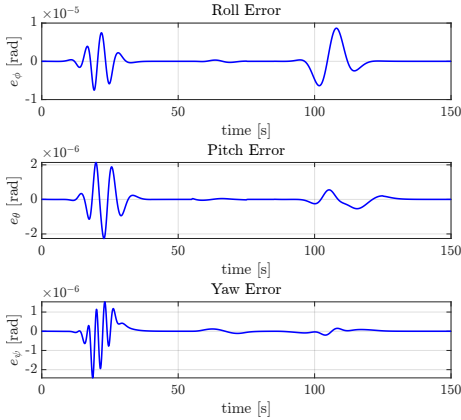
Figure 32: Roll, Pitch, Yaw Errors With Uncertainty Compensated

4) ISMC UNMATCHED DISTURBANCES: In the next case, it has been analyzed the behavior of the system under the effects of unmatched disturbance. It is essential to highlight the ISMC is able to perfectly reject just the *matched* disturbances. The disturbances acting on the system have been chosen as constant disturbances equal to: $\tau_e^b = \begin{bmatrix} 5 \cdot 10^{-2} & 5 \cdot 10^{-2} & 5 \cdot 10^{-2} \end{bmatrix}^T Nm$ and $f_e = \begin{bmatrix} 0 & 0 & 2 \end{bmatrix}^T N$. From the figures (40), (41), (42), (43) we can state that even if the system is affected by considerable disturbance, the controller is still able to track the trajectory with sufficiently small errors,

Figure 33: Linear Velocity Error With Uncertainty Compensated
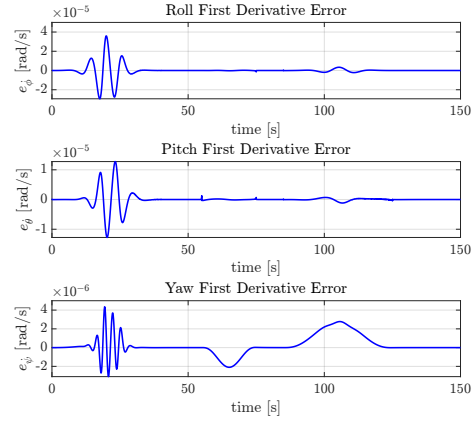
Figure 34: Roll, Pitch, Yaw First Derivatives Error With Uncertainty Compensated

Figure 35: Control Inputs With Uncertainty Compensated

which are however bigger than the first case in Figures (14), (18), (16), (20), furthermore, the transient is more
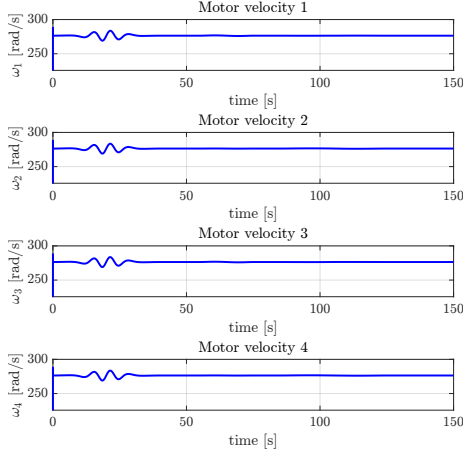
Figure 36: Norm of Propellers velocities With Uncertainty Compensated
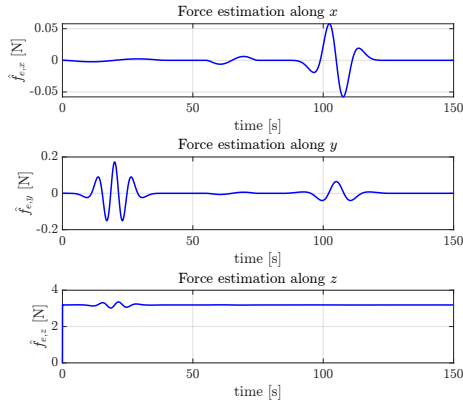
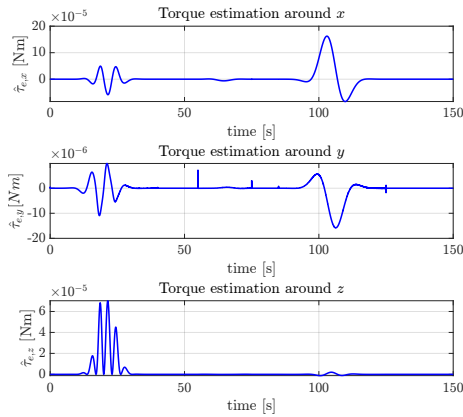Figure 37: External Forces Estimation caused by the Uncertainty

Figure 38: External Torques Estimation caused by the Uncertainty

evident. Moreover, from the figures (44) and (45) we can appreciate the differences in the control inputs and the velocities of each propeller: the thrust results much
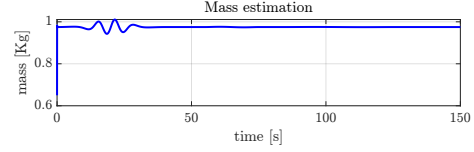

Figure 39: Mass Estimation

higher than the figure (23) and the propellers exhibit a greater rotation velocity than in Figure (24). Despite having bigger error than before, the controller is robust also with respect to unmodelled unmatched disturbances.
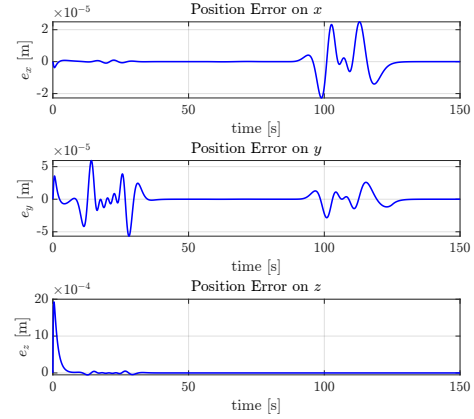
Figure 40: Linear Position Error With Disturbances
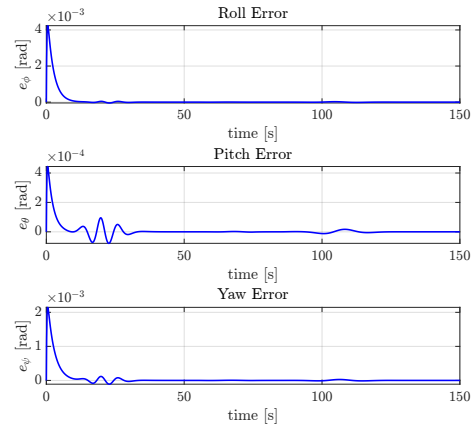
Figure 41: Roll, Pitch, Yaw Errors With Disturbances

5) ISMC + ESTIMATOR WITH UNMATCHED DISTURBANCES: As final case, let's delve into the impact of integrating the momentum-based estimator, aimed at effectively compensating for external disturbances and enhancing the controller's performance under perturbations. Upon examining figures (46), (47), (48), and (49), and comparing them with the previous case where the estimator was not employed (40), (41), (42), (43), notable differences emerge. Primarily, it becomes evident that the initial transient, required for the estimator
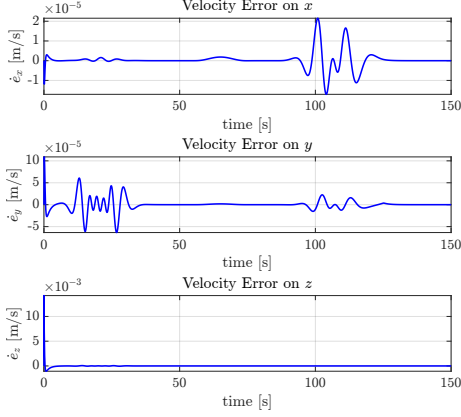
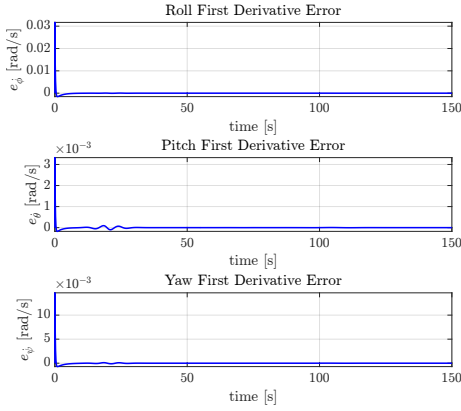Figure 42: Linear Velocity Error With Disturbances

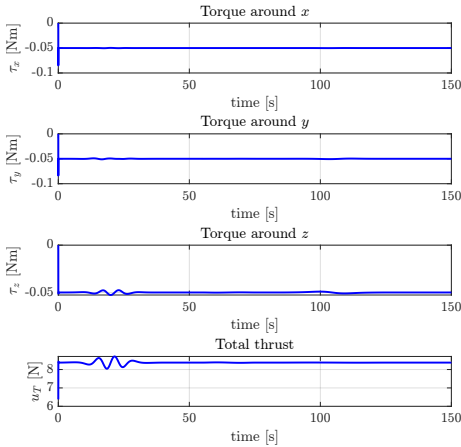Figure 43: Roll, Pitch, Yaw First Derivatives Error With Disturbances

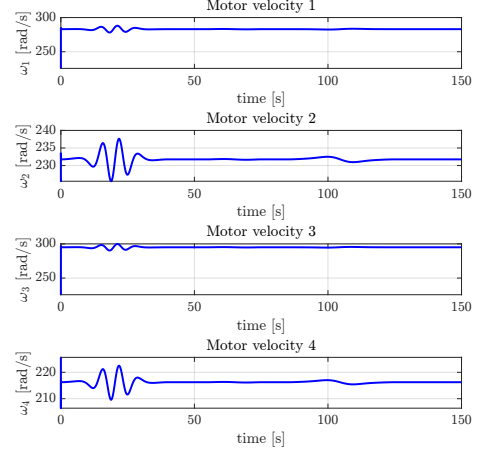Figure 44: Control Inputs With Disturbances

Figure 45: Norm of Propellers velocities With Disturbances

- the third component of the position error is drastically reduced from $20 \cdot 10^{-4}m$ to $10 \cdot 10^{-5}m$;
- the roll, pitch and yaw errors are reduced respectively from $4 \cdot 10^{-3}rad$, $4 \cdot 10^{-4}rad$, $2 \cdot 10^{-2}rad$ to $2.5 \cdot 10^{-4}rad$, $2.5 \cdot 10^{-5}rad$, $12 \cdot 10^{-5}rad$;
- the second component of linear velocity error does not exhibit an initial peak anymore;

This improvement underscores the effectiveness of the estimator in swiftly mitigating disturbances and reducing tracking errors, thus contributing to overall system stability and performance enhancement. Furthermore, in figures (52) and (53) it is possible to appreciate the efficiency of the estimation of the external wrenches.
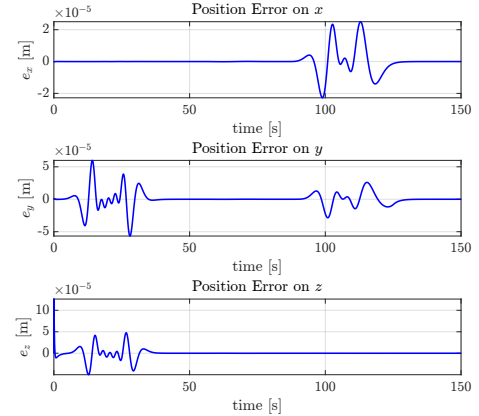

Figure 46: Linear Position Error With Disturbances Compensated

to attain steady-state estimation, is markedly reduced compared to the transient exhibited by the controller without compensation. Furthermore, the errors demonstrate a significantly lower order of magnitude with the incorporation of the estimator, indeed:

VI. CONCLUSION

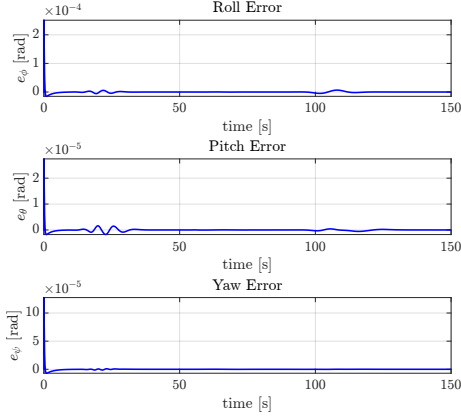From the previous results, we can conclude asserting that:

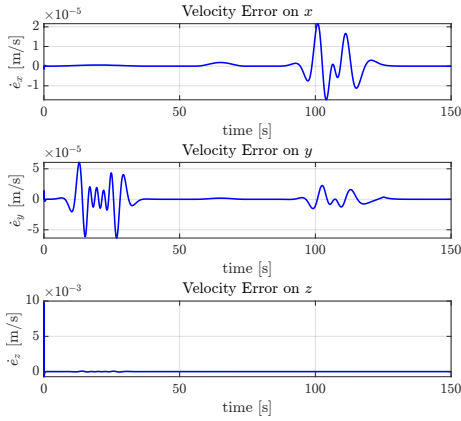Figure 47: Roll, Pitch, Yaw Errors With Disturbances Compensated

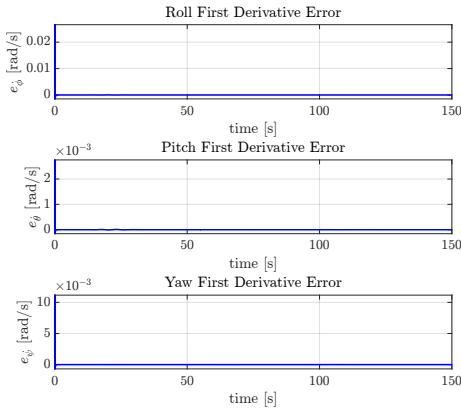Figure 48: Linear Velocity Error With Disturbances Compensated

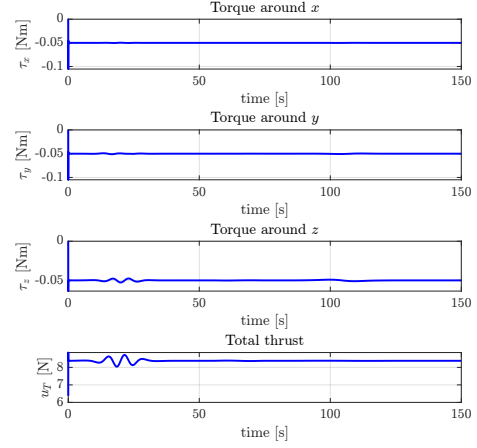Figure 49: Roll, Pitch, Yaw First Derivatives Error With Disturbances Compensated

Figure 50: Control Inputs With Disturbances Compensated
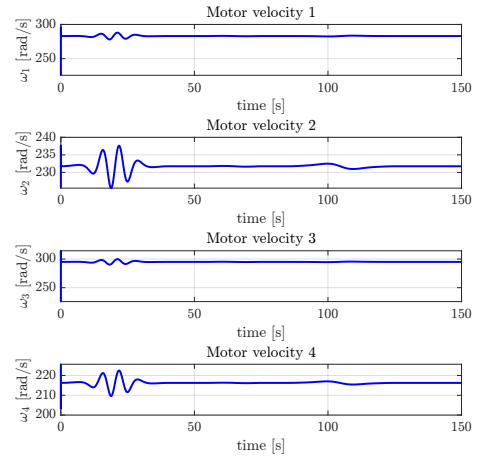
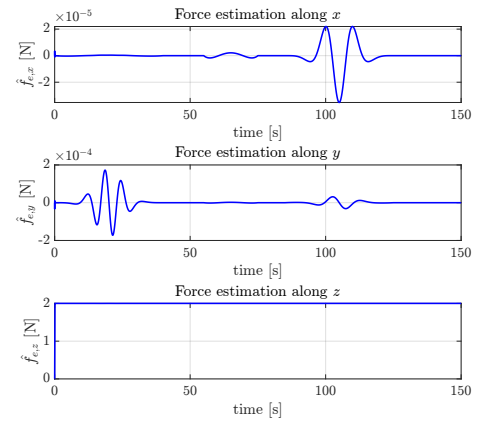Figure 51: Norm of Propellers velocities With Disturbances Compensated

Figure 52: Forces Estimation

- ISMC exhibits a robust behavior against to the uncertainties and external disturbance thanks to the sliding actions on Inner and Outer loop;
- The performances can be enhanced by considering an external wrenches estimator;
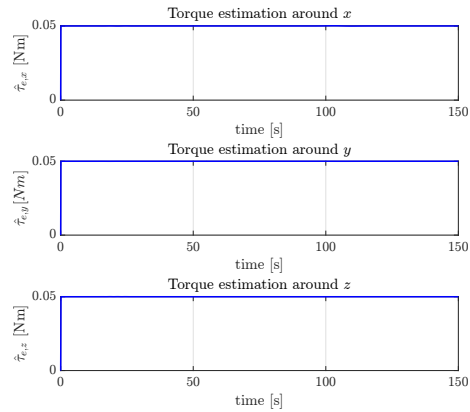- Using RPY dynamic model, the problem of repre-

Figure 53: Torques Estimation

sentation singuarities remains and could be fixed by considering a coordinate-free dynamic model;

- Gain tuning can be tough since there are a lot of parameters;
- The momentum-based estimator can affect badly the error dynamics sometimes.

References

[1] Ahmed Eltayeb et al. "Integral Adaptive Sliding Mode Control for Quadcopter UAV Under Variable Payload and Disturbance". In: *IEEE Access* 10 (2022), pp. 94754–94764. DOI: 10.1109/ACCESS. 2022.3203058.